Earth and Planetary Science Letters 438 (2016) 112–121

Contents lists available at ScienceDirect

Earth and Planetary Science Letters

www.elsevier.com/locate/epsl

A submarine landslide source for the devastating 1964 Chenega tsunami, southern Alaska

Daniel S. Brothers [a,*], Peter J. Haeussler [b], Lee Liberty [c], David Finlayson [a,1], Eric Geist [d], Keith Labay [b], Mike Byerly [e]

[a] Pacific Coastal and Marine Science Center, U.S. Geological Survey, 400 Natural Bridges Dr., Santa Cruz, CA 95060, United States
[b] Alaska Science Center, U.S. Geological Survey, 4210 University Dr., Anchorage, AK 99508, United States
[c] Boise State University, Department of Geosciences, 1910 University Dr., Boise, ID 83725, United States
[d] Pacific Coastal and Marine Science Center, U.S. Geological Survey, 345 Middlefield Rd., MS 999, Menlo Park, CA 95039, United States
[e] Alaska Department of Fish and Game, 3298 Douglas Pl., Homer, AK 99603, United States

ARTICLE INFO

Article history:
Received 13 September 2015
Received in revised form 7 January 2016
Accepted 8 January 2016
Available online 28 January 2016
Editor: P. Shearer

Keywords:
glacimarine fjord
megathrust
mass transport
paleoseismology
debris flow
inverse travel time

ABSTRACT

During the 1964 Great Alaska earthquake (M_w 9.2), several fjords, straits, and bays throughout southern Alaska experienced significant tsunami runup of localized, but unexplained origin. Dangerous Passage is a glacimarine fjord in western Prince William Sound, which experienced a tsunami that devastated the village of Chenega where 23 of 75 inhabitants were lost – the highest relative loss of any community during the earthquake. Previous studies suggested the source of the devastating tsunami was either from a local submarine landslide of unknown origin or from coseismic tectonic displacement. Here we present new observations from high-resolution multibeam bathymetry and seismic reflection surveys conducted in the waters adjacent to the village of Chenega. The seabed morphology and substrate architecture reveal a large submarine landslide complex in water depths of 120–360 m. Analysis of bathymetric change between 1957 and 2014 indicates the upper 20–50 m (~0.7 km^3) of glacimarine sediment was destabilized and evacuated from the steep face of a submerged moraine and an adjacent ~21 km^2 perched sedimentary basin. Once mobilized, landslide debris poured over the steep, 130 m-high face of a deeper moraine and then blanketed the terminal basin (~465 m water depth) in 11 ± 5 m of sediment. These results, combined with inverse tsunami travel-time modeling, suggest that earthquake-triggered submarine landslides generated the tsunami that struck the village of Chenega roughly 4 min after shaking began. Unlike other tsunamigenic landslides observed in and around Prince William Sound in 1964, the failures in Dangerous Passage are not linked to an active submarine delta. The requisite environmental conditions needed to generate large submarine landslides in glacimarine fjords around the world may be more common than previously thought.

Published by Elsevier B.V.

1. Introduction

Several sets of destructive tsunami waves were generated during and immediately after the M_w 9.2 Great Alaskan Earthquake of 1964. The devastation experienced throughout southern Alaska primarily resulted from two separate tsunami types. One was generated by the coseismic movement of the continental margin in the Gulf of Alaska, which produced long-period ocean waves that struck the Alaska coastline about 20 min after the earthquake began and propagated across the Pacific Ocean as far away as Antarctica (Plafker, 1969; Plafker et al., 1969). The second type consisted of trains of shorter period ocean waves generated locally within enclosed fjords and straits of Prince William Sound (PWS) and the Kenai Peninsula (Plafker et al., 1969; Von Huene and Cox, 1972). In many places, the local waves were catastrophic to nearshore communities and impacted the shorelines within minutes of the start of shaking. For example, the towns of Valdez, Seward and Whittier (Fig. 1; Table 1) are each located adjacent to shallow–water submerged delta fronts that failed during the earthquake. The resulting submarine landslides generated tsunami waves and significant wave runup, which severely damaged coastal infrastructure and collectively caused 54 fatalities (Haeussler et al., 2014; Parsons et al., 2014; Plafker et al., 1969; Reimnitz and Marshall, 1965; Suleimani et al., 2011; Von Huene and Cox, 1972; Wilson and Tørum, 1972). Local tsunamis were also observed in

* Corresponding author.
E-mail address: dbrothers@usgs.gov (D.S. Brothers).
[1] Now at: Chesapeake Technology, 1605 El Camino Real, Mountain View, CA 94040, United States.

http://dx.doi.org/10.1016/j.epsl.2016.01.008
0012-821X/Published by Elsevier B.V.

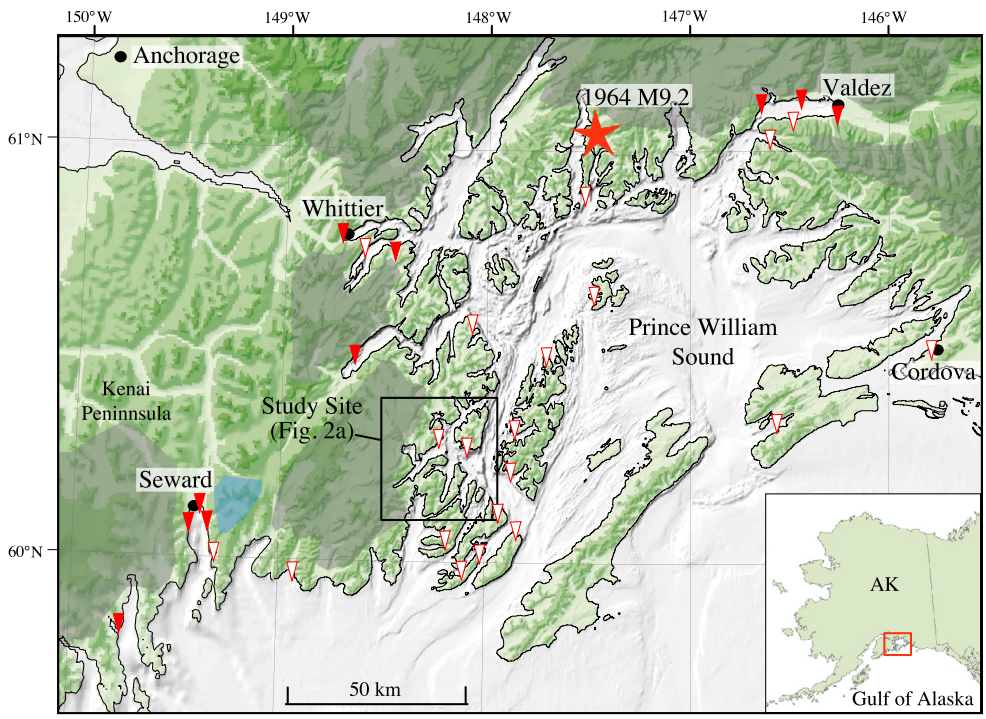

Fig. 1. Shaded relief map of Prince William Sound and surrounding region. Triangles are documented locations of high wave runup during the 1964 Great Alaskan Earthquake (red star marks the epicenter). Observed runup linked to a submarine landslide is filled red; runup of unexplained origin is filled white (following Fig. 2 of Nicolsky et al., 2013); runup observations are from Plafker et al. (1969). Gray shaded regions are locations of large ice fields and active glaciation (e.g., Wiles et al., 1999). (For interpretation of the references to color in this figure legend, the reader is referred to the web version of this article.)

Table 1
Sites of documented landslide-induced tsunami runup.

Location	Fatalities	Max runup (m)	Landslide volume (km^3)	References
Whittier	13	32	0.04	Haeussler et al. (2014), Plafker et al. (1969)
Valdez	33	67	0.4–1.0	Lee et al. (2007), Parsons et al. (2014), Plafker et al. (1969)
Seward	13	12	0.2	Haeussler et al. (2007), Plafker et al. (1969), Wilson and Tørum (1972)
Chenega	23	21	0.1–0.7	This study, Plafker et al. (1969)

many other places in and around PWS (white triangles in Fig. 1), but the specific source mechanisms remain unknown (Plafker et al., 1969; Von Huene and Cox, 1972; Nicolsky et al., 2013). The importance of delineating the sources of these events is highlighted by the fact that a total of 82 lives were claimed in 1964 by local tsunamis, but also because many high-latitude commercial ports and coastal communities are located along glacimarine fjords. Most documented landslides in fjord settings occur in relatively shallow water along submerged delta fronts, depositional environments known to be prone to failure during earthquakes and other transient sources of shear stress (e.g., Aarseth et al., 1989; Hampton et al., 1996; L'Heureux et al., 2010; Lastras et al., 2013; St-Onge et al., 2004; Syvitski and Schafer, 1996; Prior et al., 1982, 1986; Reimnitz and Marshall, 1965). Nevertheless, most fjords lack the data needed to systematically evaluate the potential hazards.

One of the most devastating, but poorly understood local tsunamis of 1964 struck the native village of Chenega in western PWS (Fig. 2). Waves virtually destroyed the village, and 23 of 75 inhabitants lost their lives (KPIX-TV, 1964; Plafker et al., 1969). Surviving residents were temporarily relocated to other townships until 1984 when 'New' Chenega was reestablished in Sawmill Bay, ∼20 km to the south of the original site (Nicolsky and Koehler, 2014). Although eyewitnesses helped document the sequence of events at Chenega in 1964 (Plafker et al., 1969), the specific source of the destructive waves remains heretofore unknown. We present new interpretations of the tsunami source based on high-resolution marine geophysical data acquired in the waters near Chenega. Our results help constrain tsunami hazards across southern Alaska and provide new insights into submarine landslide occurrence and associated tsunami generation in glacimarine fjords.

2. Background

Dangerous Passage is one of several glacially eroded fjords that extends westward of Knight Island Passage and contains a series of smaller elongate tributary fjords, including Icy Bay, Whale Bay, Jackpot Bay and Nassau Fjord (Fig. 2a). Late Pleistocene glaciers retreated from PWS into the headland fjords around 10,000 yr B.P. (Barclay et al., 2009). The most recent major ice advance in southern Alaska occurred during the late Little Ice Age (LIA; Barclay et al., 2009), in which many of the ice margins advanced to their Holocene maxima (Calkin et al., 2001). Princeton Glacier, located to the west of Nassau Bay, is thought to have merged with Chenega and Tigertail glaciers during the LIA and advanced to the mouth of Nassau Bay, before retreating back to the fjord head in the late 1800s (Wiles et al., 1999). The heads of Nassau Bay and Icy Bay still contain tidewater glaciers. Several rudimentary (by today's standards) bathymetric surveys of Dangerous Passage and surrounding inlets were conducted since 1950, but there has been no detailed marine geological study of this area.

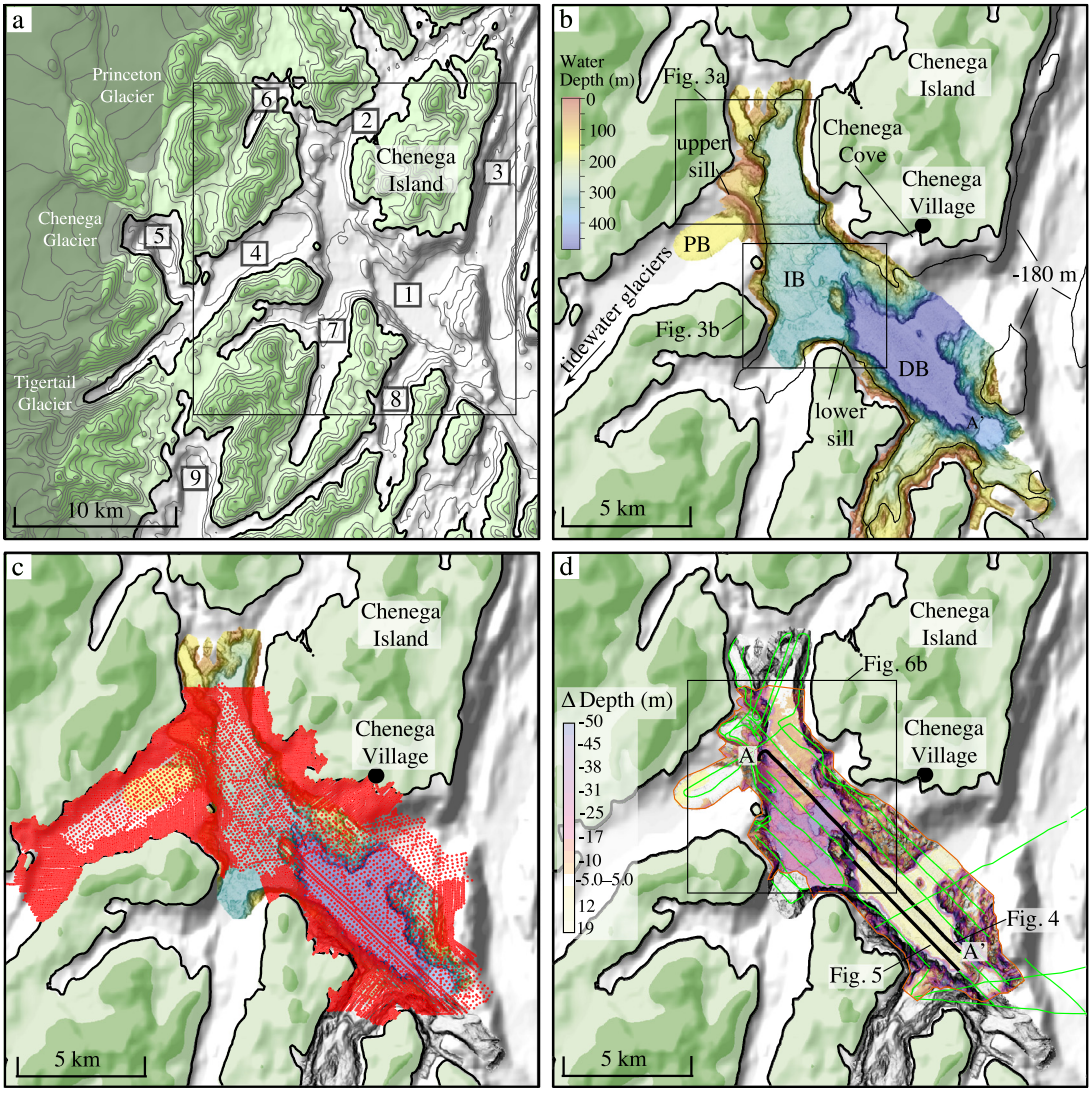

Fig. 2. (a) Southern Dangerous Passage and surrounding tributary fjords. Contours on land have 100 m intervals; offshore contours have 20 m intervals. Labels include (1) Southern Dangerous Passage, (2) Northern Dangerous Passage, (3) Knight Island Passage, (4) Icy Bay, (5) Nassau Bay, (6) Jackpot Bay, (7) Whale Bay, (8) Bainbridge Passage, and (9) Port Bainbridge. Shaded relief data are from multiple datasets: two from the National Geophysical Data Center, including multibeam bathymetry data from NOAA survey H11388 (Sinson, 2004) and from a 8/3 arc-second (∼100 m) resolution coastal relief model of Prince William Sound (Caldwell et al., 2011). Black square is extent of (b–d). (b) High-resolution shaded relief multibeam bathymetry data (colored region is extent of 2014 data), including the 180 m (∼100 fathom) depth contour. The seabed can be geomorphically separated into a proximal basin (PB), intermediate basin (IB), and distal basin (DB). Black squares are enlarged sections in Figs. 3(a, b). (c) Digitized soundings from NOAA 1957 hydrographic surveys (Natella, 1957a, 1957b). Soundings were used to estimate bathymetric change from 1957 to 2014 (see methods section). (d) Results of elevation differencing between 1958 and 2014; changes in depth are color-coded and draped on the 2014 shaded relief bathymetry as semi-transparent overlay. Positive/negative values show places where the 2014 water depth is shallower/deeper than 1958, respectively. Green lines represent seismic reflection profiles; black lines are the locations of the seismic reflection profiles in Figs. 4 and 5, as well as the bathymetric profile shown in Fig. 6(a). (For interpretation of the references to color in this figure legend, the reader is referred to the web version of this article.)

The original village of Chenega, located on the southern shore of Chenega Island (Fig. 2b), was the site of a devastating tsunami that struck shortly after the earthquake began on March 27th, 1964 (Plafker et al., 1969; Von Huene and Cox, 1972). At the time, the water level in Dangerous Passage was at ∼0.3 m above the mean lower low water datum (Wilson and Tørum, 1972). The following section, taken directly from Plafker et al. (1969), describes the sequence of events that occurred at Chenega.

> The earthquake shaking, which began gently but became much stronger within 1 minute, lasted an estimated 4 1/2 to 5 minutes… between 60 and 90 seconds after shaking began the first wave rose quietly but rapidly about half way up the beach. It receded rapidly almost at once, exposing the floor of the entire cove to an estimated depth of 20 or more fathoms and for a distance of about 300 yards offshore. A second and much higher wave arrived within 4 minutes of the earthquake's onset and before shaking had ceased. This wave, which was about 35 feet high, ran up to the schoolhouse foundation, a height of 70 feet. All the buildings except one house and the school were either smashed into the trees or swept out to sea with the backwash… waves comparable in size to those at Chenega struck elsewhere along the coast of the island, particularly in the cove just east of Chenega. There, most of the muskeg and all of the trees were stripped from the surface; blocks of bedrock were even torn from a 20-foot seacliff.

Runup patterns in Chenega Cove and the three coves to the east (Fig. 2b) suggested the wave came from the southwest (Plafker et al., 1969). Although Plafker et al. (1969) noted the possibility for the waves to have been caused by a sizable submarine landslide, fathometer profiles indicated that no significant changes in

bathymetry occurred in water depths shallower than 180 m following the earthquake (see contour in Fig. 2b), an early observation used to argue against a major proximal submarine landslide as the source of the tsunami. According to Plafker et al. (1969) most of the shoreline around Dangerous Passage consists of exposed bedrock and there are no significant masses of unconsolidated sediment that may have failed during the earthquake. Coseismic uplift of Chenega Island was 1.5 m according to tide gauge measurements and horizontal displacement was approximately 17 m to the southeast (Plafker, 1969). Regional tsunami models focused on regional coseismic uplift and subsidence as tsunami sources, but struggled to reproduce eyewitness observations and severely underestimated the magnitude of wave runup in many places around PWS (Johnson et al., 1996; Ichinose et al., 2007; Suito and Freymueller, 2009). Furthermore, documented evidence for coseismic surface faulting is more than 20 km to the southeast of Chenega (e.g., Plafker, 1967; Haeussler et al., 2015). Subsequent models included the effects of both horizontal and vertical coseismic deformation, which produced better alignment with eyewitness reports, but still underestimated the runup in and around Dangerous Passage (Nicolsky et al., 2013). For more than fifty years the true source of the devastating tsunami remained unclear.

3. Data and methods

In May 2014, the U.S. Geological Survey (USGS) led a marine geophysical survey offshore Chenega Village aboard the Alaska Department of Fish and Game vessel *R/V Solstice*. A primary objective was to acquire high-resolution bathymetric and subbottom imagery and conduct comparative analysis between the new data and hydrographic surveys conducted prior to the 1964 earthquake. Approximately 65 km^2 of multibeam bathymetry data were acquired with a Reson SeaBat 7111 (100 kHz; 301 beams). Tide values were referenced to Mean Lower Low Water and soundings were edited and processed using Reson PDS2000 software. A final raster grid was created at 10-m cell spacing and loaded into ESRI ArcGIS and QPS Fledermaus for interpretation (e.g., Fig. 2b) and comparison to bathymetric data acquired in 1957 (Fig. 2c).

The U.S. Coast and Geodetic Survey conducted bathymetric surveys in Dangerous Passage and surrounding waters in 1957 (Natella, 1957a, 1957b). Vessel positioning was obtained through triangulation to control stations using U.S. Navy hydrographic sextants and soundings were referenced to Mean Lower Low Water based on measurements from a portable tide gage placed on Chenega Island. The resulting smooth sheet bathymetric charts were projected into NAD27 UTM Zone 6N. A total of 18,207 depth soundings on the smooth sheets were digitized, interpolated and gridded in ArcGIS, then reprojected into NAD83 Zone 6N (Fig. 2c). Surface differencing between 1957 data and 2014 data (Fig. 2d) was used to identify bathymetric change following the approach applied to other fjords of the region (Haeussler et al., 2007, 2014; Parsons et al., 2014). Note both bathymetric data sets were referenced to Mean Lower Low Water datum and differencing estimates account for ∼1.4 m of coseismic uplift that occurred in 1964. However, absolute uncertainties in the 1957 data are not available largely due to the amount of bathymetric change that occurred in the time period between 1957 and 2014. Errors are expected to be low in areas that have a relatively flat seafloor and higher in places having substantial variation and relief (e.g., Haeussler et al., 2007). We assume that any bathymetric change of ±5 m is within the uncertainty envelope. The bathymetric differencing grid was draped on the 2014 shaded relief bathymetry as color-coded and semi-transparent values; this allowed direct comparison between changes in depth with morphological features observed in the 2014 data (e.g., scarps, channels and debris aprons).

Additionally, 160 line-km of high-resolution single-channel seismic reflection profiles were acquired in 2014 using a 500 J SIG 2-Miile minisparker source (Fig. 2d). Acoustic frequencies were concentrated between 140–350 Hz, providing ∼3–5 m vertical resolution and penetration of up to 500 ms (300–400 m). Data were processed using Sioseis and loaded into IHS Kingdom Suite software for interpretation. Modern depositional models for glacimarine fjords provide examples of sedimentary processes active in proximal environments, and illustrate how these processes control the spatial distribution of sediment delivery and deposition (Cai et al., 1997; Carlson, 1989; Cowan and Powell, 1990; Powell, 1984; Syvitski and Shaw, 1995), as well as morphological features associated with submarine landslides (e.g., Aarseth et al., 1989; Lee et al., 2006; Syvitski and Schafer, 1996; Syvitski and Shaw, 1995). As such, seismic facies interpretations are used to identify evidence for erosion/deposition that may be linked to changes in water depth during the timeframe of 1957–2014.

Finally, inverse travel-time modeling was performed for qualitative comparison to eyewitness observations at Chenega Village. Calculations of tsunami travel-times are based on the linear long-wave assumption for phase speed (Mei et al., 2005), using the Geoware TTT software described by Wessel (2009). An 8/3 arc-sec bathymetric DEM (Caldwell et al., 2011) was used to generate travel-time estimates. Typically, inverse travel-time modeling uses the arrival time at multiple observation stations to constrain the location and dimension of the source (Hatori, 1966; Hirata et al., 2003; Ishii et al., 2013). In our application, because we have only one observation station in the Chenega region, an N-min travel-time contour marks all possible initiation points of a hypothetical tsunami that takes N-min to reach the shoreline at Chenega Village. Integrated analyses of seabed morphology, substrate architecture, eyewitness reports and tsunami travel-time curves are used to explore the true source(s) of the destructive 1964 tsunami.

4. Results

4.1. Seabed morphology and substrate architecture

Stepped sedimentary basins separated by bathymetric sills and bounded by steep, rugged slopes characterize the first-order morphology of lower Dangerous Passage (Figs. 2 and 3). The most prominent (upper) sill is a narrow, arcuate ridge ∼5 km-long and between 50–70 m water depth (Figs. 2 and 3). The sill has ∼100 m of relief on its stoss-side flank (i.e., nearest the glacial source) and up to 220 m of relief on its lee-side flank. The sill separates Icy Bay, the proximal basin, from southern Dangerous Passage, the intermediate and distal basins. The deeper half of the lee-side flank is covered by several short (>1 km), arcuate seabed scarps having greater than 20 m of relief (Fig. 3a). Similar features are also observed to the north of the sill along a series of small bathymetric embayments. The largest scarps face east/southeast and display up to 100 m of relief (labeled "major scarps" in Figs. 3a, b). Between the upper and lower sills is an elongate, intermediate basin spanning water depths of 260–360 m and an area of ∼21 km^2. Despite its gentle slope (∼1.5°) the intermediate basin floor is rough, hummocky, and covered by arcuate scarps of highly variable length and height, broad scarp-bounded depressions, lobate features of positive relief, and subtle channels and pits (Fig. 3a). Intact blocks of material (50–250 m across) are observed adjacent to and downslope of scarps (Fig. 3b). Blocks and scarps are visible along the edge of the multibeam data coverage in Whale Bay, suggesting such features continue at least another kilometer into Whale Bay.

The lower sill separates the intermediate basin from a deeper, distal basin. Total relief between the two basins is ∼130 m. The sill includes what may be a bedrock outcrop near its midpoint and its

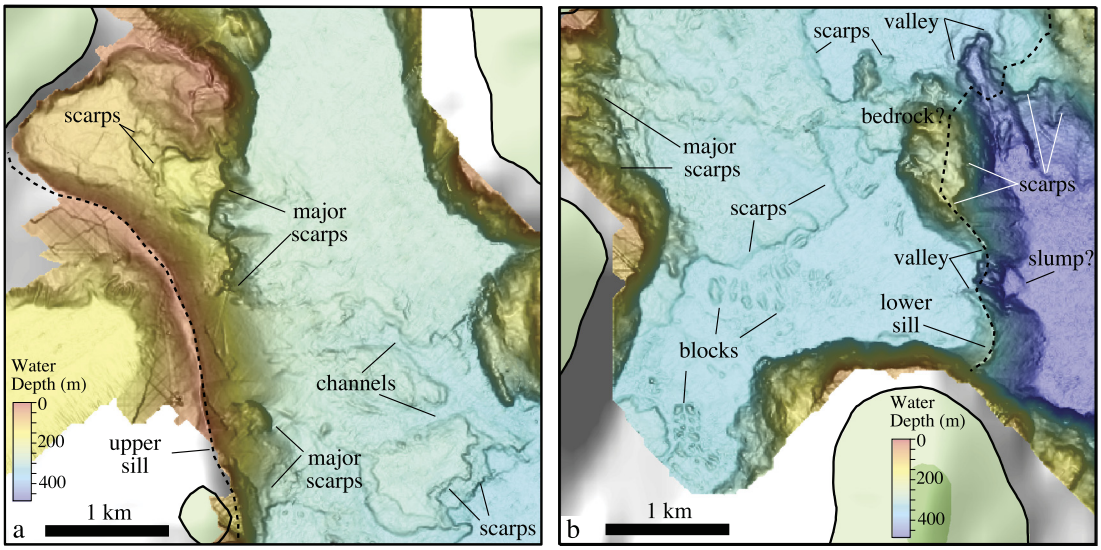

Fig. 3. Enlarged regions of high-resolution shaded relief bathymetry data acquired in 2014. See Fig. 2b for relative locations. Dashed black lines follow the crests of the upper and lower bathymetric sills.

lee-side flank contains several irregular scarps (Fig. 3b). The scarps display at least 20 m of relief, but relatively limited spatial extent. Two sections of the sill have negative relief with respect to the adjacent basin floor and appear to be disrupted or breached by erosional scour and incision associated with steep valleys that connect the two basins (Fig. 3b). Finally, the seafloor of the distal basin is virtually flat at a nearly uniform water depth of 460–480 m. The basin floor is ∼14 km^2 (estimated using new multibeam data and data from the 8/3 arc-second Coastal Relief Model of Caldwell et al., 2011).

The intermediate and distal basins contain relatively thick sequences of sedimentary fill bounded by rugged, high-amplitude acoustic basement (Fig. 4). The basement interface is inferred to be the contact between bedrock or massively bedded glacial moraine deposits and the overlying glacimarine sedimentary fill. The intermediate basin contains at least six wedge-shaped sediment packages (Fig. 4), ranging from 20 to 40 m-thick. Each package appears to onlap the buried flanks of the sills and basin margins (i.e., acoustic basement) and contains highly variable internal seismic character. Near the lee-side of the upper sill, internal reflectors show a mostly chaotic pattern. Moving basinward, the chaotic character grades into an irregular reflector pattern and then into sub-parallel reflector stratification. Some of the uppermost packages show a chaotic internal reflector pattern and are truncated along highly irregular bounding surfaces and seabed scarps; in some cases, basal surfaces exposed at the foot of the scarps are an extension of continuous reflectors buried farther upslope (e.g., 'slip surface' in Fig. 4b).

The sedimentary fill of the distal basin is greater than 250 m thick (Fig. 4). With the exception of the reflector packages in the uppermost 20 m, the continuity of reflectors and degree of stratification is greater in the distal basin than the intermediate basin. The uppermost package appears to contain at least two distinctive sub-units. A buried, lenticular-shaped unit no more than 10 m thick is observed along the northwestern reach of the distal basin and proximal to the base of the lower sill, but pinches out to the southeast (see "localized landslide deposit" in Figs. 4b and 5). The overlying unit is characterized by weak and discontinuous internal reflectors and is observed throughout the distal basin. Both units rest upon an irregular, high-amplitude basal surface, which appears to truncate underlying parallel reflectors (Fig. 4b inset; Fig. 5). This basal surface was picked on all profiles and interpolated to generate a 3-D surface throughout the lower basin. Assuming a p-wave velocity of 1500 m/s that is typical of water saturated marine sediment, the average thickness of the sediment emplaced above the basal surface is 13 ± 5 m. Horizons below the basal surface and proximal to the lower sill are discontinuous, display variable amplitude, and contain some chaotic internal reflectors. Basinward of the lower sill, the same packages grade into semi-continuous and parallel reflectors of variable amplitude (Fig. 4b inset; Fig. 5).

Bathymetric differencing between 2014 and 1957 reveals dramatic differences in the seabottom (Figs. 1d, 6a, b): (1) the intermediate basin is deeper in 2014 than in 1957 by an average of 21 ± 12 m and 30–50 m deeper across broad patches of seafloor; (2) the distal basin is shallower by an average of 11 ± 5 m, slightly less than the estimated thickness of the sediment above the basal surface identified in the seismic profiles. The scarps along the lee side of the upper sill are associated with significant deepening, as are both valleys along the distal face of the lower sill. However, it is difficult to constrain the absolute bathymetric change along the sill flanks because errors in the differencing are presumably greatest in places that are steep and rugged.

4.2. Tsunami travel-time estimates

Comparison between inverse tsunami travel-time estimates in southern Dangerous Passage and the underlying seabed morphology help link eyewitness observations to potential tsunami source regions (Fig. 6c). Most of the scarps, blocks, channels and valleys of the intermediate basin, described above, are located within the 3-min travel-time contour. Some of the major scarps along the lee-side face of the upper sill roughly align the 3-min contour; other scarps near the northern extent of the multibeam data, as well as potential scarps beyond the multibeam coverage in Whale Bay, roughly align with the 4-min contour. The region between the 1- and 2-min contours contains the 180 m depth contour (i.e., the maximum depth of offshore surveys mentioned in Plafker et al., 1969) as well as some of the scarps along the face the lower sill. The seafloor within the 1-min contour (e.g., Chenega Cove) is outside the new multibeam data coverage.

5. Geological interpretations

The sedimentary processes operating during and after the most recent major ice advance typically control sediment accumulation in fjords (Syvitski and Shaw, 1995) and include a combination

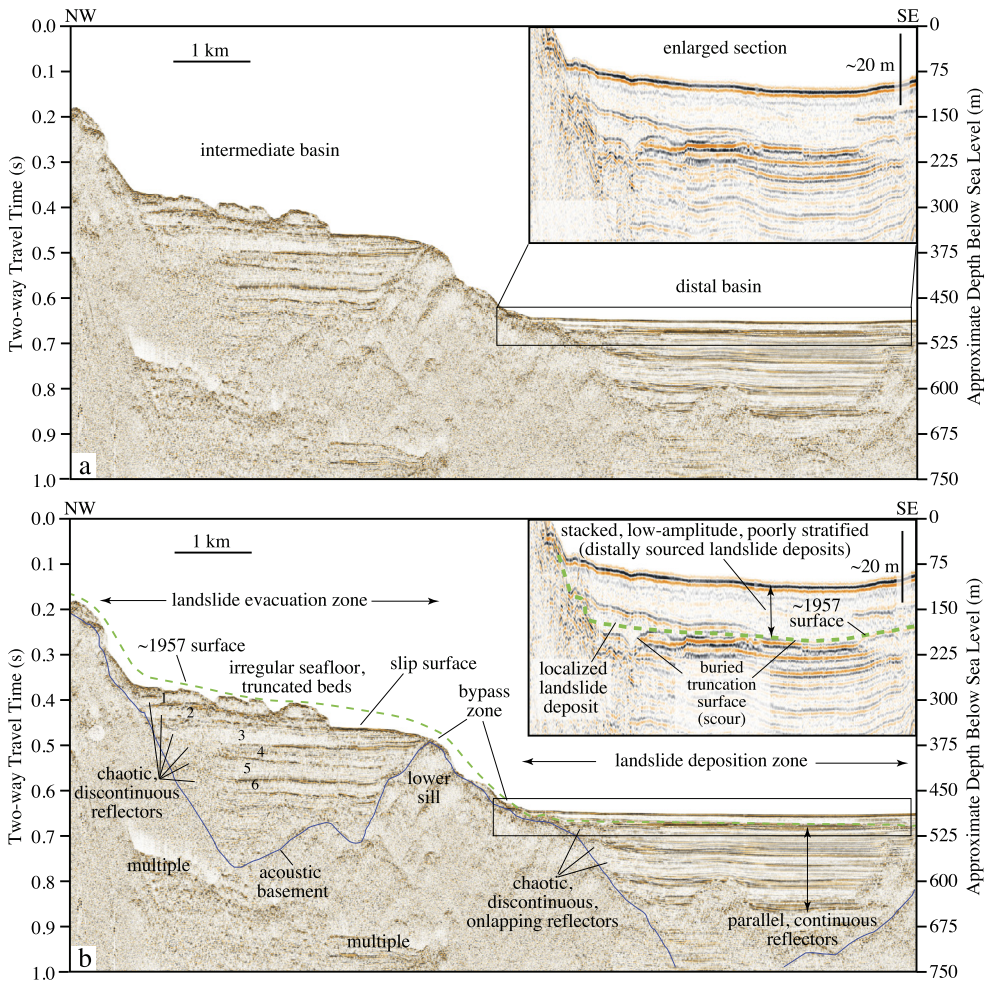

Fig. 4. (a) Seismic reflection profile spanning the intermediate and distal basins (see Fig. 2d for location). Approximate depth is estimated assuming a constant velocity of 1500 m/s. (b) Interpreted section highlighting geologic and geomorphic features, including failure scarps in the intermediate basin and landslide deposits in the distal basin. The dashed green line marks the approximate depth of the seafloor in 1957 (i.e., prior to the earthquake and tsunami). (For interpretation of the references to color in this figure legend, the reader is referred to the web version of this article.)

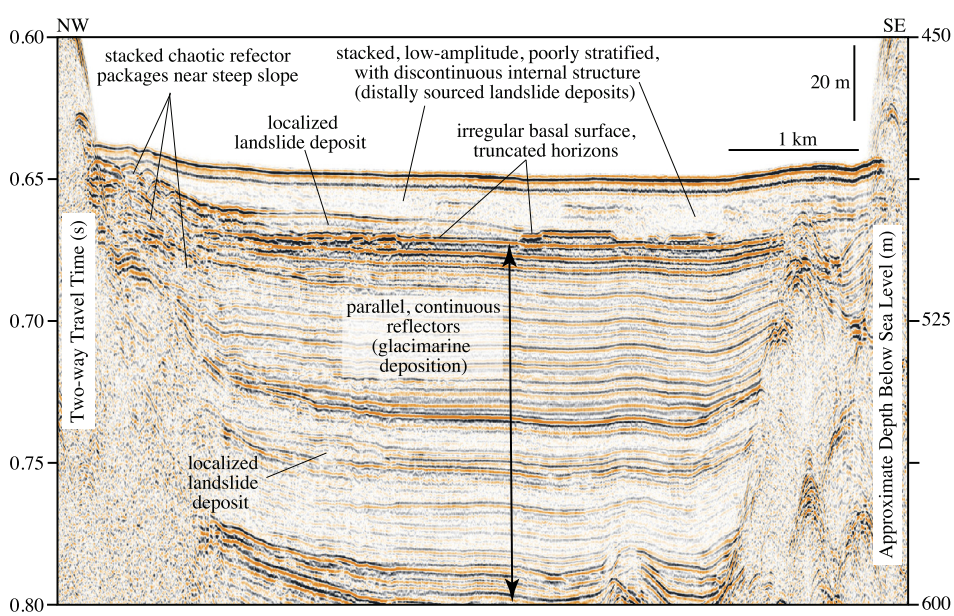

Fig. 5. Seismic reflection profile spanning the distal basin (see Fig. 2d for location). Note the dramatic difference in seismic character between the units located above and below the basal truncation surface. Also, we observe a deeper, localized landslide deposit at about 0.74 s two-way travel time. Presumably this older failure was similar to the localized failure that occurred in 1964.

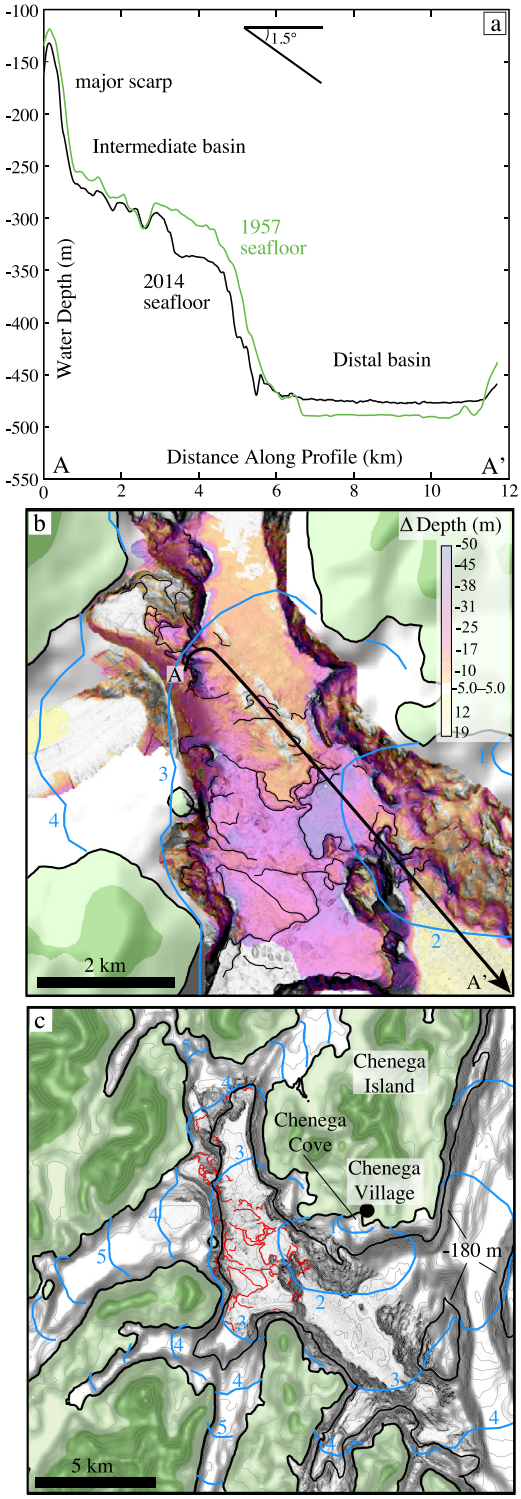

Fig. 6. (a) 2-D bathymetric profiles of extracted from the 1957 surface and from the 2014 surface (profile location is shown in Fig. 2d). (b) Detailed image of bathymetric change along the intermediate basin and the lee-side flanks of the upper and lower bathymetric sills (see Fig. 2d for relative location). Changes in depth are color-coded and draped on the 2014 shaded relief bathymetry as semi-transparent overlay. Transparent patches represent 0 ± 5 m change and black lines are submarine landslide scarps. Note the correlation between seafloor scarps in the shaded relief imagery and areas of significant change in seafloor depth. (c) Inverse tsunami travel time estimates (blue contours of contour number N denote all possible initiation points of a hypothetical tsunami that takes N-min to reach the shoreline at Chenega Village), 180 m depth contour (black line) and landslide scarps (red lines). Note wave travel time estimates do not consider the time involved with the landslide initiation process. (For interpretation of the references to color in this figure legend, the reader is referred to the web version of this article.)

of (a) proximal glacimarine sediments characterized by interbedded sediment flow and hemipelagic deposits, and (b) fine-grained distal glacimarine sediments. Fjords located in and around Prince William Sound contain steep slopes and receive abundant sediment of highly variable grain size, making them ideal environments to generate submarine landslides and sediment flows (Hampton et al., 1996; Lee et al., 2006). Because fine-grained and under-consolidated glacimarine sediment is characteristically susceptible to strength loss during earthquakes (e.g., Schwab and Lee, 1983; Schwab et al., 1987; Syvitski and Schafer, 1996), triggered slides may accelerate quickly depending on slope angle and generate tsunamis. In general, most tsunamigenic mass movements involve predominantly fine-grained sediment, therefore the viscoplastic fluid model for muddy debris flows is a central model for tsunami generation (e.g., Locat et al., 2009). A clay content of only 10% or more is needed for debris flows to be adequately modeled by viscoplastic rheology (Coussot, 1997; Coussot and Meunier, 1996).

At present, the heads of Icy Bay and Nassau Fjord (Fig. 2a) contain tidewater glaciers and continue to deliver a significant volume of proximal glacimarine sediment to Icy Bay (Wiles et al., 1999). It is possible that mid- to late-Holocene ice advances extended the length of Icy bay, likely as far seaward as the upper sill, which appears to be the terminal moraine enclosing Icy Bay (Fig. 3a). We expect a significant volume of fine-grained, distal glacimarine sediment to be transported from Icy Bay into Dangerous Passage and surrounding inlets via tidal currents. Given the high-frequency nature of the sparker seismic source, the depth of acoustic penetration in both basins (>250 m) is impressive and implies sedimentary fill is predominantly fine-grained (i.e., low impedance and signal attenuation). The irregular and internally discordant sedimentary packages stacked in the intermediate basin are inferred to be mass transport deposits sourced from repeated failures of glacimarine sediment originally deposited along the lee-side flank of the upper bathymetric sill. Hence the dominant mode of sediment emplacement in the intermediate basin since glaciers receded out of Dangerous Passage appears to be from submarine landslides. Based on the number of distinctive packages imaged in the intermediate basin, there appear to have been at least six episodes of failure and deposition. The curvature and slope of the seabed in 1957 (e.g., Figs. 4b and 6a) suggest that the shallowmost package(s) emplaced in the intermediate basin exceeded the basin capacity and began to prograde toward the rim of the lower sill. Thus a broad, ∼20–50 m thick lens of unstable sediment became perched ∼120 m above the floor of the distal basin. High rates of Holocene glacimarine sedimentation throughout Dangerous Passage (particularly during the Little Ice Age), emplacement of fine-grained deposits along the steep slopes of the fjord margins, and apparent progradation of the intermediate basin are a few of the requisite preconditioning factors for submarine landslide generation.

The seabed morphology observed throughout the intermediate basin is characteristic of a major submarine landslide complex (Mulder and Cochonat, 1996) and has several features in common with failures observed in other fjords (Haeussler et al., 2007, 2014; L'Heureux et al., 2010; Lee et al., 2006; Prior et al., 1982, 1986). Successive headwall scarps, sidewall scarps, transported blocks and complex patterns of channelization suggest that a set of coalescing failures evacuated significant portions of the shallowest 50 m of the basin. Four distinctive patches of seafloor show 20–55 m of deepening from 1957–2014 (Fig. 7). Two of the patches are along the lee-side of the upper moraine; the other two are bounded by headwall and sidewall scarps and appear to have failed along a stratigraphic surface that most likely represented a plane of weakness (e.g., Fig. 4).

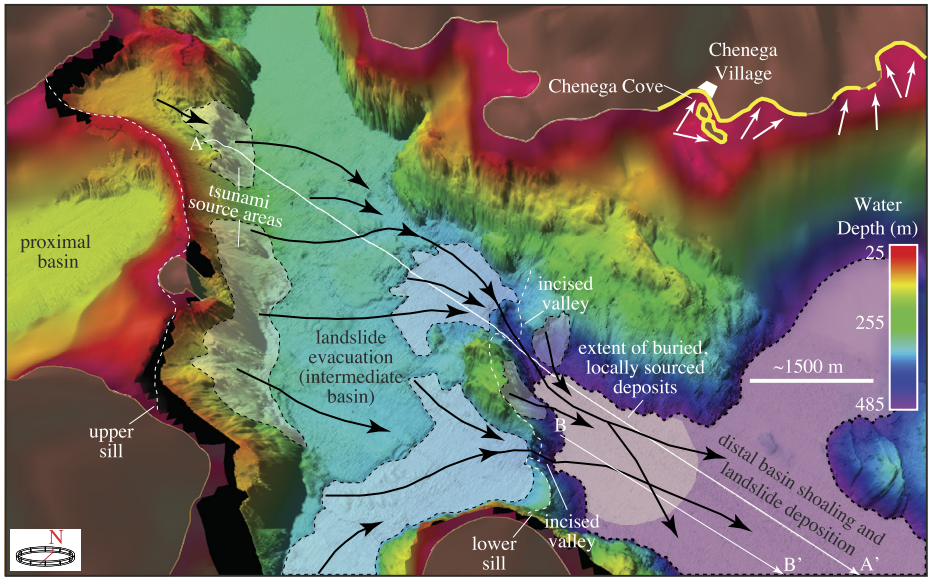

Fig. 7. 3-D perspective view of shaded relief bathymetry offshore Chenega village. Shaded patches of seafloor depict areas that experienced dramatic changes in water depth between 1957 and 2014. Patches within the intermediate basin are sites of sediment evacuation and deepening (∼21 m); the floor of the distal basin is a site of sediment deposition and shoaling (∼11 m). Black arrows are interpreted sediment flow pathways. Flows sourced from the failure along upper sill and intermediate basin eroded valleys into the steep face of the lower sill; the resulting deposits blanketed the distal basin and were emplaced on top of a localized landslide deposit (imaged in Figs. 4 and 5) that was probably sourced from nearby failures along the face of the lower sill. White arrows indicate the inferred 1964 tsunami travel direction and yellow lines mark areas surrounding Chenega Village that experienced significant tsunami runup (from Plafker et al., 1969). Profiles A–A′ and B–B′ are shown in Figs. 4 and 5. (For interpretation of the references to color in this figure legend, the reader is referred to the web version of this article.)

The morphological and stratigraphic character of the distal basin is dramatically different than that of the intermediate basin. The scarps along the lee-side face of the lower sill (also a moraine separating the intermediate and distal basins) suggest a proximal source for some landslide deposits in the distal basin. The buried, lenticular-shaped deposit above the basal surface (Figs. 4 and 5) and adjacent to the base of the lower sill is probably an example of a deposit sourced from nearby failures along the steep face of the lower sill (Fig. 7). The irregular morphology along the basal horizon and associated evidence for truncated reflectors (Figs. 4b inset and 5) suggest these locally sourced landslides deformed and eroded the floor of distal basin, including the 1957 surface. We propose that the collapse of under-consolidated sediment in the intermediate basin and along the lee-side flank of the upper sill led to coalescing debris flows that spilled over the steep relief of the lower sill and into the distal basin. We interpret the overlying, poorly stratified unit to be the terminal landslide deposit sourced primarily from material evacuated from the intermediate basin (Fig. 4 inset; Fig. 5), although there may be inter-bedded deposits of local origin that are not resolved in the available data. Failed sections of the intermediate basin were transported up to 5.5 km before reaching the rim of the lower sill.

After failure, landslides traversing steep slopes often develop into a succession of sediment flows that erode channels into the underlying surfaces (e.g., Syvitski et al., 1987). The lower sill is incised by two bathymetric valleys (Figs. 3b and 7), which suggests the landslides evacuated from the intermediate basin accelerated and became highly erosive sediment flows as they traversed the steep, lee-side flank of the lower moraine (see bypass zone in Fig. 4). The virtual absence of discernable seabed morphology and the poorly developed internal structure associated with the post-1957 deposits in the distal basin also suggests that sediment flows reaching the basin floor were of relatively low density and viscosity, and thus spread out along the basin floor up to 6 km away from the lower sill, filling it to a nearly constant depth. Plafker et al. (1969) noted significant numbers of red snapper, typically found near the seabed of deeper waters, were found dead at the surface near Chenega immediately after the 1964 earthquake. It is likely that earthquake-triggered submarine landslides and associated sediment flows killed the fish.

Finally, the character of the landslide deposits in the upper 20 m of the distal basin is dramatically different than the underlying units, which appear to be dominated by glacimarine sedimentation typical of deep-water fjords (e.g., Powell, 1984; Syvitski et al., 1987). There is definitive evidence for only one small and localized failure deposit in the deeper, pre-1964 sedimentary section (Fig. 5). However, most of the layers below the basal unconformity have an apparent basinward progression from discontinuous and chaotic reflector character near the base of the lower sill to subparallel/parallel stratification farther basin-ward (Figs. 4 and 5). This suggests some of the background sediment accumulation in the distal basin is linked to small landslides that experienced flow transformation over a relatively short distance (1–2 km) from their sources. The total volume of the landslide deposits above the basal unconformity is between 0.09–0.24 km^3; however, landslide deposits appear to have also been emplaced in the intermediate basin, making this a minimum volume estimate for sediment mobilized since 1957. The deepening of the intermediate basin (-21 ± 12 m) implies that up to 0.7 km^3 of sediment was evacuated since 1957.

The widespread evidence for changes in seafloor depth due to slope failure, landslide generation and mass transport deposition between 1957 and 2014, and inverse travel time modeling make an earthquake triggered submarine landslide a compelling source for the tsunami that destroyed Chenega Village. Nearly all of the morphological evidence for slope failure occurs deeper than the 180 m depth contour (Fig. 2b), the depth limit of bathymetric surveys conducted after 1964 tsunami (see description in Plafker et al., 1969). Despite our limited constraints on the exact timing of slope failure, the total volume of sediment transferred between the basins and the character of the resulting slide deposit suggest that most of the mass transport occurred during a punctuated event that was easily capable of generating a large tsunami wave. Assuming the 1964 earthquake triggered all of the geomorphic change between 1957 and 2014, then the volume of material mobilized by the earthquake is comparable to that for tsunamigenic landslides

observed in fjords offshore Seward, Valdez and Whittier (Fig. 1; Table 1), except that the failures occurred in significantly greater water depths and have no connection to shallow water deltas (Fig. 7). The 1964 deposits appears to be the only volumetrically significant mass transport deposit emplaced in the distal basin (Figs. 4 and 5), which suggests its source region, the intermediate basin, was uniquely primed for failure when the earthquake struck (relative to its configuration during previous large earthquakes in the region). As noted previously, increased sediment delivery during and immediately after the Little Ice Age likely set the stage for slope failure in Dangerous Passage, as well as several other fjords of southern Alaska.

6. Revisiting the 1964 Chenega tsunami

The inverse tsunami travel-time estimates (Fig. 6c) and new geomorphic observations necessitate that the sequence of events witnessed by village residents be revisited. The possible source region for the initial smaller (1–2 m) wave that struck Chenega 1–1.5 min after shaking began is only partially covered by the new high-resolution bathymetric data. The seafloor between the 1- and 2-min contours contains scarps and evidence for failure along the lower sill (Figs. 3b, 6c and 7), which may have generated the small wave. Alternatively, this initial wave may have been generated by purely coseismic vertical and horizontal ground displacement as described by Nicolsky et al. (2013). The larger catastrophic wave that struck Chenega ∼4 min after shaking began can be qualitatively matched with a number of potential submarine landslide source areas, most notable are the large headwall scarps along the steep flank of the upper moraine (Figs. 3a, 6c and 7). A large, fast moving slump or rotational landslide may have generated a southeast-directed catastrophic wave sometime during the first minute of shaking, as observed near Seward, Valdez and Whittier in the 1964 earthquake. The mass failure may have resulted in subsequent destabilization of other sections of the intermediate basin. However, because the flanks of the upper moraine and sediment deposited in the intermediate basin appear to have been preconditioned for failure and contain complexes of coalescing failure scarps, it is difficult to isolate a specific tsunami source.

Tsunami wave speed equals $\sqrt{gd}$ in the long-wavelength limit, where g is gravitational acceleration and d is water depth. Therefore, because of the water depths offshore Chenega, the large southeast-directed water wave would probably outrun similarly directed debris flows, particularly across the intermediate basin because of the low slope angle. As debris flows traversed the intermediate basin and spilled over the edge of the lower sill, they would have accelerated rapidly down the 20° slope, and thus generate additional sources of waves. Finally, in any landslide scenario, retrogressive failure and continued destabilization of seafloor may have continued several hours or days after the initial event, creating additional surges and waves.

7. Conclusions

The 1964 Great Alaska Earthquake triggered submarine landslides and locally sourced tsunamis in several fjords of Prince William Sound, but several places experienced significant runup of uncertain origin including Chenega Island (Fig. 7; Plafker et al., 1969; Nicolsky et al., 2013; Von Huene and Cox, 1972). High-resolution marine geophysical data provide the basic starting point needed to identify and characterize the processes capable of generating local tsunamis. Our results suggest that rapid sediment accumulation in the intermediate basin led to the development of a perched sedimentary basin less than 2 km offshore Chenega Village. Between 20–50 m of unstable sediment was evacuated by a complex of submarine landslides during the earthquake. There was also significant mass wasting of the lee-side face of the upper moraine, which was the probable source of the destructive tsunami that impacted the village of Chenega roughly 4 min after shaking began. These results imply that submarine landslides are a likely source for unexplained runup throughout southern Alaska (e.g., Von Huene and Cox, 1972), and may be an overlooked hazard for fjords globally (e.g., Aarseth et al., 1989; Lastras et al., 2013; Prior et al., 1982; St-Onge et al., 2004; Syvitski and Schafer, 1996). Lastly, future studies involving targeted sediment coring would help constrain the lithology, geotechnical properties and age of mass transport deposits in Dangerous Passage. Such data could provide information needed to develop morphodynamic models of submarine landslide complexes originating in glacimarine fjords and assess their associated tsunami generation mechanisms.

Acknowledgements

The USGS Coastal and Marine Geology Program and the Alaska Department of Fish and Game provided support for this project. We would like to thank the captain and crew of the R/V Solstice, as well as Gerry Hatcher, Alicia Balster-Gee, Jared Kluesner and Roland Von Huene. Amy East, David Tappin and Jason Patton provided helpful reviews. Any use of trade, product, or firm names is for descriptive purposes only and does not imply endorsement by the U.S. Government.

References

Aarseth, I., Lønne, Ø., Giskeødegaard, O., 1989. Submarine slides in glaciomarine sediments in some western Norwegian fjords. Mar. Geol. 88, 1–21.

Barclay, D.J., Wiles, G.C., Calkin, P.E., 2009. Holocene glacier fluctuations in Alaska. Quat. Sci. Rev. 28 (21), 2034–2048.

Cai, J., Powell, R.D., Cowan, E.A., Carlson, P.R., 1997. Lithofacies and seismic-reflection interpretation of temperate glacimarine sedimentation in Tarr Inlet, Glacier Bay, Alaska. Mar. Geol. 143 (1), 5–37.

Caldwell, R.J., Eakins, B.W., Lim, E., 2011. Digital elevation models of Prince William Sound, Alaska: procedures, data sources and analysis. Edited by U.S. Department of Commerce, NOAA Technical Memorandum NESDIS NGDC-40, Boulder, CO.

Calkin, P.E., Wiles, G.C., Barclay, D.J., 2001. Holocene coastal glaciation of Alaska. Quat. Sci. Rev. 20 (1), 449–461.

Carlson, P.R., 1989. Seismic reflection characteristics of glacial and glacimarine sediment in the Gulf of Alaska and adjacent fjords. Mar. Geol. 85 (2), 391–416.

Coussot, P., Meunier, M., 1996. Recognition, classification and mechanical description of debris flows. Earth-Sci. Rev. 40, 209–227.

Coussot, P., 1997. Mudflow Rheology and Dynamics. Balkema, Rotterdam, 255 pp.

Cowan, E.A., Powell, R.D., 1990. Suspended sediment transport and deposition of cyclically interlaminated sediment in a temperate glacial fjord, Alaska, USA. Geol. Soc. (Lond.) Spec. Publ. 53 (1), 75–89.

Haeussler, P.J., Lee, H.J., Ryan, H.F., Labay, K., Kayen, R.E., Hampton, M.A., Suleimani, E.N., 2007. Submarine slope failures near Seward, Alaska, during the M9.2 1964 earthquake. In: Lykousis, V., Sakellariou, D., Locat, J. (Eds.), Submarine Mass Movements and Their Consequences. Springer, New York, pp. 269–278.

Haeussler, P.J., Parsons, T., Finlayson, D.P., Hart, P.E., Chaytor, J.D., Ryan, H., Lee, H., Labay, K., Peterson, A., Liberty, L., 2014. New imaging of submarine landslides from the 1964 earthquake near Whittier, Alaska, and a comparison to failures in other Alaskan fjords. In: Krastel, S., et al. (Eds.), Submarine Mass Movements and Their Consequences. Springer, New York, pp. 361–370.

Haeussler, P.J., Armstrong, P.A., Liberty, L.M., Ferguson, K.M., Finn, S.P., Arkle, J.C., Pratt, T.L., 2015. Focused exhumation along megathrust splay faults in Prince William Sound, Alaska. Quat. Sci. Rev. 113, 8–22. http://dx.doi.org/10.1016/j.quascirev.2014.10.013.

Hampton, M.A., Lee, H.J., Locat, J., 1996. Submarine landslides. Rev. Geophys. 34 (1), 33–59. http://dx.doi.org/10.1029/95rg03287.

Hatori, T., 1966. Vertical displacement in a tsunami source area and the topography of the sea bottom. Bull. Earthq. Res. Inst. 44, 1449–1464.

Hirata, K., Geist, E.L., Satake, K., Tanioka, Y., Yamaki, S., 2003. Slip distribution of the 1952 Tokachi–Oki earthquake (M 8.1) along the Kuril Trench deduced from tsunami waveform inversion. J. Geophys. Res., Solid Earth 108. http://dx.doi.org/10.1029/2002JB001976.

Ichinose, G., Somerville, P., Thio, H.K., Graves, R., O'Connel, D., 2007. Rupture process of the 1964 Prince William Sound, Alaska, earthquake from the combined inversion of seismic, tsunami, and geodetic data. J. Geophys. Res., Solid Earth 112. http://dx.doi.org/10.1029/2006JB004728.

Ishii, M., Kiser, E., Geist, E.L., 2013. Mw 8.6 Sumatran earthquake of 11 April 2012: rare seaward expression of oblique subduction. Geology 41, 319–322.
Johnson, J.M., Satake, K., Holdahl, S.R., Sauber, J., 1996. The 1964 Prince William Sound earthquake: joint inversion of tsunami and geodetic data. J. Geophys. Res., Solid Earth 101 (B1), 523–532. http://dx.doi.org/10.1029/95jb02806.
KPIX-TV, 1964. Chenega is gone. In: Hubbard, R., Pussey, R., Williams, D. (Eds.), San Francisco Bay Area Television Archive. San Francisco State University. https://diva.sfsu.edu/collections/sfbatv/bundles/189328, accessed June 3, 2015.
L'Heureux, J.S., Hansen, L., Longva, O., Emdal, A., Grande, L., 2010. A multidisciplinary study of submarine landslides at the Nidelva fjord delta, Central Norway – implications for geohazard assessment. Norwegian J. Geol. 90 (1–2), 1–20.
Lastras, G., Amblas, D., Calafat, A.M., Canals, M., Frigola, J., Hermanns, R.L., Lafuerza, S., Longva, O., Micallef, A., Sepúlveda, S.A., 2013. Landslides cause tsunami waves: insights from Aysén Fjord, Chile, Eos. Trans. Am. Geophys. Union 94 (34), 297–298.
Lee, H., Ryan, H., Kayen, R.E., Haeussler, P.J., Dartnell, P., Hampton, M.A., 2006. Varieties of submarine failure morphologies of seismically-induced landslides in Alaskan fjords. Norwegian J. Geol. 86 (3), 221–230.
Lee, H.J., Ryan, H.F., Haeussler, P.J., Kayen, R.E., Hampton, M.A., Locat, J., Suleimani, E., Alexander, C.R., 2007. Reassessment of seismically induced, tsunamigenic submarine slope failures in Port Valdez, Alaska, USA. In: Lycousis, V., Sakellarion, D., Locat, J. (Eds.), Submarine Mass Movements and Their Consequences. Springer, Dordrecht, pp. 357–365.
Locat, J., Lee, H., ten Brink, U., Twichell, D.C., Geist, E.L., Sansoucy, M., 2009. Geomorphology, stability and mobility of the Currituck slide. Mar. Geol. 264 (1), 28–40.
Mei, C.C., Stiassnie, M., Yue, D.K.-P., 2005. Theory and Applications of Ocean Surface Waves. Part 1: Linear Aspects. World Scientific, Singapore, 513 pp.
Mulder, T., Cochonat, P., 1996. Classification of offshore mass movements. J. Sediment. Res. 66 (1), 43–57.
Natella, F., 1957a. Hydrographic survey south of Chenega Island, Prince William Sound, Alaska. Report to the U.S. Department of Commerce, 26 pp.
Natella, F., 1957b. Hydrographic survey south of Dangerous Passage, Prince William Sound, Alaska. Report to the U.S. Department of Commerce, 26 pp.
Nicolsky, D.J., Suleimani, E.N., Hansen, R.A., 2013. Note on the 1964 Alaska tsunami generation by horizontal displacements of ocean bottom. Numerical modeling of the runup in Chenega Cove, Alaska. Pure Appl. Geophys. 170 (9–10), 1433–1447.
Nicolsky, D.J., Koehler, R.D., 2014. Tsunami inundation maps of the villages of Chenega Bay and northern Sawmill Bay, Alaska. Alaska Division of Geological and Geophysical Surveys Report of Investigation 2014-3, 50 pp.
Parsons, T., Geist, E.L., Ryan, H.F., Lee, H.J., Haeussler, P.J., Lynett, P., Hart, P.E., Sliter, R., Roland, E., 2014. Source and progression of a submarine landslide and tsunami: the 1964 Great Alaska earthquake at Valdez. J. Geophys. Res., Solid Earth 119 (11), 8502–8516.
Plafker, G., 1967. Surface faults on Mantague Island associated with the 1964 Alaska Earthquake. U.S. Geological Survey Professional Paper 543-G, 41 p., 2 sheets, scales 1:31,680 and ∼1:20,000, http://pubs.usgs.gov/pp/0543g/.
Plafker, G., 1969. Tectonics of the March 27, 1964, Alaska earthquake. U.S. Geological Survey Professional Paper 543-I, 74 p., 2 sheets, scales 1:2,000,000 and 1:500,000, http://pubs.usgs.gov/pp/0543i/.
Plafker, G., Kachadoorian, R., Eckel, E.B., Mayo, L.R., 1969. Effects of the earthquake of March 27, 1964 on various communities. U.S. Geological Survey Professional Paper 542-G, 43 p., 2 sheets, scales 1:2,500,000 and 1:250,000, http://pubs.usgs.gov/pp/0542g/.
Powell, R.D., 1984. Glacimarine processes and inductive lithofacies modelling of ice shelf and tidewater glacier sediments based on Quaternary examples. Mar. Geol. 57 (1), 1–52.
Prior, D.B., Bornhold, B.D., Coleman, J.M., Bryant, W.R., 1982. Morphology of a submarine slide, Kitimat Arm, British Columbia. Geology 10, 588–592.
Prior, D.B., Bornhold, B.D., Johns, M.W., 1986. Depositional characteristics of a submarine debris flow. J. Geol. 92 (6), 707–727.
Reimnitz, E., Marshall, N.F., 1965. Effects of the Alaska earthquake and tsunami on recent deltaic sediments. J. Geophys. Res. 70 (10), 2363–2376.
Schwab, W.C., Lee, H.J., 1983. Geotechnical analyses of submarine landslides in glacial marine sediment, northeast Gulf of Alaska. In: Molnia, B.F. (Ed.), Glacial-Marine Sedimentation. Springer, New York, NY, pp. 145–184.
Schwab, W.C., Lee, H.J., Molnia, B.F., 1987. Causes of varied sediment gravity flow types on the Alsek prodelta, northeast Gulf of Alaska. Mar. Geotechnol. 7, 317–342.
Sinson, D.A., 2004. Descriptive report to accompany hydrographic survey H11388: N.E. Bainbridge Passage. Report to the U.S. Department of Commerce, National Oceanic and Atmospheric Administration, 26 pp.
St-Onge, G., Mulder, T., Piper, D.J.W., Hillaire-Marcel, C., Stoner, J.S., 2004. Earthquake and flood-induced turbidites in the Saguenay Fjord (Québec): a Holocene paleoseismity record. Quat. Sci. Rev. 23 (3–4), 283–294.
Suito, H., Freymueller, J.T., 2009. A viscoelastic and afterslip postseismic deformation model for the 1964 Alaska earthquake. J. Geophys. Res., Solid Earth 114. http://dx.doi.org/10.1029/2008jb005954.
Suleimani, E., Nicolsky, D.J., Haeussler, P.J., Hansen, R., 2011. Combined effects of tectonic and landslide-generated tsunami runup at Seward, Alaska during the Mw 9.2 1964 earthquake. Pure Appl. Geophys. 168 (6–7), 1053–1074.
Syvitski, J.P., Burrel, D.C., Skei, J.M., 1987. Fjords: Processes and Products. Springer-Verlag New York Inc., New York, NY, 379 pp.
Syvitski, J.P., Shaw, J., 1995. Sedimentology and geomorphology of fjords. Dev. Sedimentol. 53, 113–178.
Syvitski, J.P., Schafer, C.T., 1996. Evidence for an earthquake-triggered basin collapse in Sagenay Fjord, Canada. Sediment. Geol. 104, 127–153.
Von Huene, R., Cox, D.C., 1972. Locally generated tsunamis and other local waves. In: The Great Alaska Earthquake of 1964: Oceanography and Coastal Engineering. National Academy of Sciences, Washington, DC, pp. 211–221.
Wessel, P., 2009. Analysis of observed and predicted tsunami travel times for the Pacific and Indian Oceans. Pure Appl. Geophys. 166, 301–324.
Wiles, G.C., Barclay, D.J., Calkin, P.E., 1999. Tree-ring-dated 'Little Ice Age' histories of maritime glaciers from western Prince William Sound, Alaska. Holocene 9 (2), 163–173.
Wilson, B.W., Tørum, A., 1972. Effects of the tsunamis: an engineering study. In: The Great Alaska Earthquake of 1964: Oceanography and Coastal Engineering. National Academy of Sciences, Washington, DC, pp. 361–523.